Langmuir

ARTICLE

pubs.acs.org/Langmuir

Control of Superhydrophilicity/Superhydrophobicity using Silicon Nanowires via Electroless Etching Method and Fluorine Carbon Coatings

Beom Seok Kim, Sangwoo Shin, Seung Jae Shin, Kyung Min Kim, and Hyung Hee Cho*

Department of Mechanical Engineering, Yonsei University, 262, Seongsanno, Seodaemun-gu, Seoul 120-749, Korea

S Supporting Information

Downloaded via SEOUL NATL UNIV SCIENCE & TECHLGY on June 19, 2021 at 05:40:16 (UTC).
See https://pubs.acs.org/sharingguidelines for options on how to legitimately share published articles.

ABSTRACT:

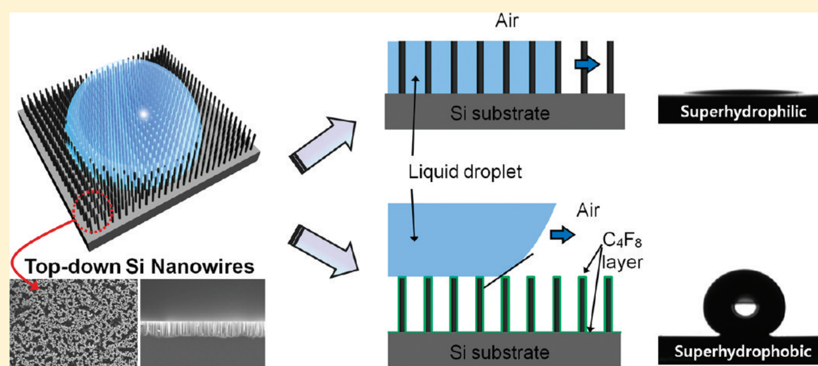

Surface roughness is promotive of increasing their hydrophilicity or hydrophobicity to the extreme according to the intrinsic wettability determined by the surface free energy characteristics of a base substrate. Top-down etched silicon nanowires are used to create superhydrophilic surfaces based on the hemiwicking phenomenon. Using fluorine carbon coatings, surfaces are converted from superhydrophilic to superhydrophobic to maintain the Cassie−Baxter state stability by reducing the surface free energy to a quarter compared with intrinsic silicon. We present the robust criteria by controlling the height of the nanoscale structures as a design parameter and design guidelines for superhydrophilic and superhydrophobic conditions. The morphology of the silicon nanowires is used to demonstrate their critical height exceeds several hundred nanometers for superhydrophilicity, and surpasses a micrometer for superhydrophobicity. Especially, SiNWs fabricated with a height of more than a micrometer provide an effective means of maintaining superhydrophilic (<10°) long-term stability.

INTRODUCTION

Modifying surface wettability is important in diverse fields, including physics, chemistry, biology, and engineering. There have been many studies on the effects of surface wettability on fluid mechanics and heat transfer.[1−7] When a surface is hydrophobic, fluidic performance can be enhanced by decreasing the pressure drop, because a hydrophobic surface diminishes the skin friction caused by the interaction between a solid surface and a liquid stream.[1,3,7,8] It has also been reported that superhydrophobic characteristics can be used to produce a waterproof self-cleaning surface that mimics a lotus leaf.[9−14] On the other hand, hydrophilic and superhydrophilic surfaces have been employed to enhance the performance of boiling heat transfer.[4,5,15] In particular, the critical heat flux (CHF, a general standard for boiling heat transfer performance) of a superhydrophilic surface has recently been improved to about twice that of a plain (unmodified) surface.[5] Applications of superhydrophilic surfaces include biomolecular purification and an antifogging technology, based on liquid imbibition[16,17] drug delivery, and a low-temperature fuel cell system to prevent the conglomeration of liquid byproducts, which causes performance degradation by choking or flooding.[18,19]

A considerable amount of research on various applications has been focused on fabricating superhydrophilic or superhydrophobic surfaces by controlling the surface free energy (SFE) and roughness, using a TiO_2 coating layer,[10,13,20] micronanoscale structure fabrication,[21−26] based on analytical approaches via geometrical morphology control.[27−29] However, some of the previous studies are subject to a number of limitations for use in practical applications. First, the procedures must be compatible with designing and creating practical devices, while providing the simplicity, robustness, and cost/labor control demanded in fabrication processes. Moreover, it should be possible and clear to present specific design guidelines to manipulate the wettability by controlling related variables, such as SFE and surface roughness.[30−36]

Received: March 12, 2011
Revised: July 5, 2011
Published: July 06, 2011

ACS Publications © 2011 American Chemical Society

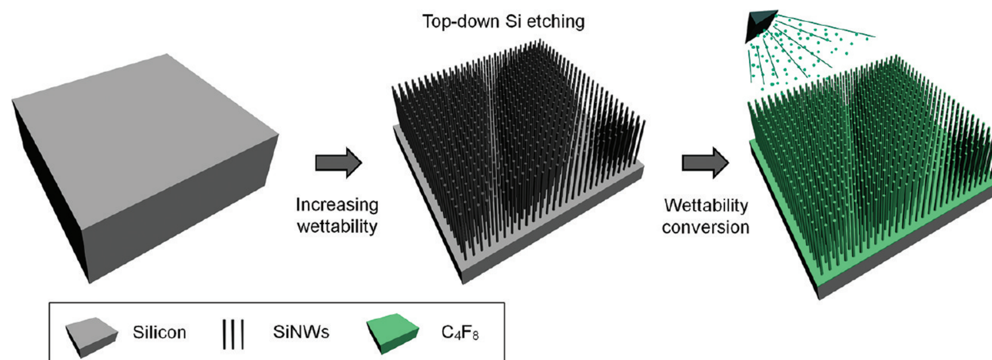

Figure 1. Schematic of the fabrication processes for increasing hydrophilicity and converting hydrophilic/superhydrophilic surfaces into hydrophobic/superhydrophobic surfaces.

In this study, we present a simple and robust fabrication process for superhydrophilic/superhydrophobic surfaces using the electroless silicon etching (EE) method[37,38] and C_4F_8 polymer coating. The synthesis of rough silicon nanowire arrays (SiNWs) via the EE method is a well-known top-down technique that can be used to modify the morphology of a surface with nanoscale structures over a large area in a room-temperature environment. The technique is used in this study, because it enables the surface roughness to be readily maximized with SiNWs of high aspect ratio. Although there is little research on the realization of superhydrophilic and superhydrophobic surfaces using SiNWs via the EE method, this study would present the feasible manipulation of wettability and the prerequisite conditions with designing guidelines for the robust surfaces. Using densely distributed vertical SiNWs with a height of more than a micrometer, it is possible to create an extremely rough surface, in specific a prerequisite of structural dimensions for fabricating superhydrophilic/superhydrophobic surfaces. For the conversion of wettability from superhydrophilic to superhydrophobic, we used the PECVD technique, a common polymer layer deposition process. We demonstrate that theoretical criteria for the manipulation of wettability and the robustness characteristics can be satisfied by controlling the surface free energy of the substrate and the surface roughness factor. On the basis of the theoretical evaluation for the robust surface design, we then present design guidelines that conform to permissible height requirements for SiNWs to create superhydrophilic/superhydrophobic surfaces. In addition, for the long-term stability of the surfaces, we are to demonstrate the characteristics of the surfaces and present potential approaches.

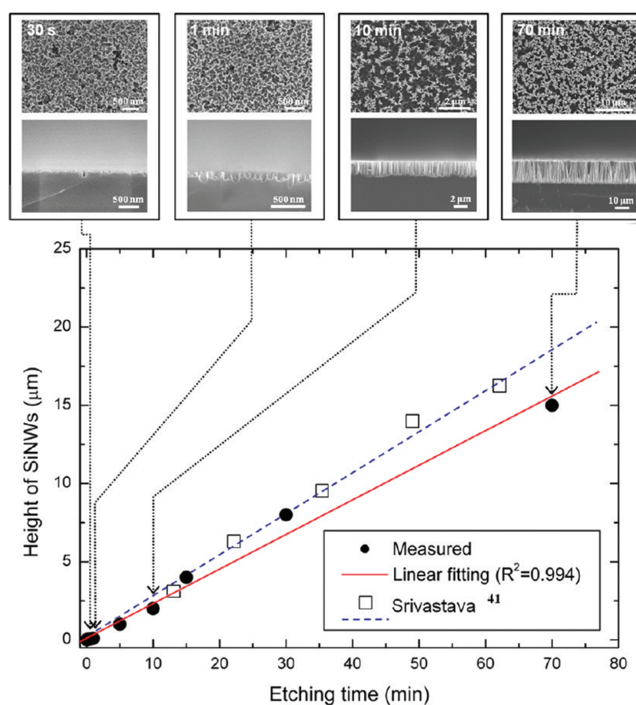

Figure 2. Scanning electron microscopy (SEM) images of SiNWs synthesized by electroless etching for various etching times, showing the height dependence of the SiNWs on etching time. Black circles indicate average SiNW heights measured by SEM, and the red solid line represents is a linear trend.

EXPERIMENTAL SECTION

Synthesis of SiNWs Using Electroless Silicon Etching and C_4F_8 Deposition. Using top-down electroless silicon etching, we roughened silicon surfaces by adding densely distributed vertical SiNWs. In this study, we used 4-in. n-type (phosphorus-doped) silicon wafers with 500-μm thickness, (100) orientation, and resistivity between 1 and 10 Ω cm. First, the wafer was cleaned for 40 min in a mixture of H_2SO_4 and H_2O_2 solutions with a volume ratio of 3:1. This was followed by an additional cleaning step, using a sonicator with acetone and methanol in turn for more than 5 min each. To synthesize the SiNWs, each wafer was immersed in etching solution (a mixture of 0.02 M $AgNO_3$ and 5 M HF) at room temperature, and the etching time was varied to control the height of the SiNWs. In this step, Ag^+ ions dissolved in the etching solution attach themselves to the silicon surface by galvanic displacement. The silicon surface in contact with the Ag^+ ions undergoes oxidization to become SiO_2, and then the locally formed oxides are etched by the hydrofluoric acid. As the etching process progresses, the remaining silicon becomes the vertical SiNWs. During the etching step, Ag^+ ions continue to grow on the surface and form dendrite structure.[39] The etched silicon substrate was cleaned for 80 min to remove the Ag dendrite structures, using nitride acid (70%) at room temperature. Finally, the substrates with the SiNWs were immersed in DI water to rinse the surface, and then dried by natural convection under ambient conditions.

The polymeric C_4F_8 layer was deposited by PECVD, using a deep-trench reactive ion etcher system (Multiplex, Surface Technology System), which is generally used in a Bosch process.[40] For hydrophobic surfaces, we deposited the polymeric layer on the samples under conformal deposition condition of 20 nm thickness on a plain surface. For the deposition, we used PECVD-equipment (Multiplex, Surface Technology

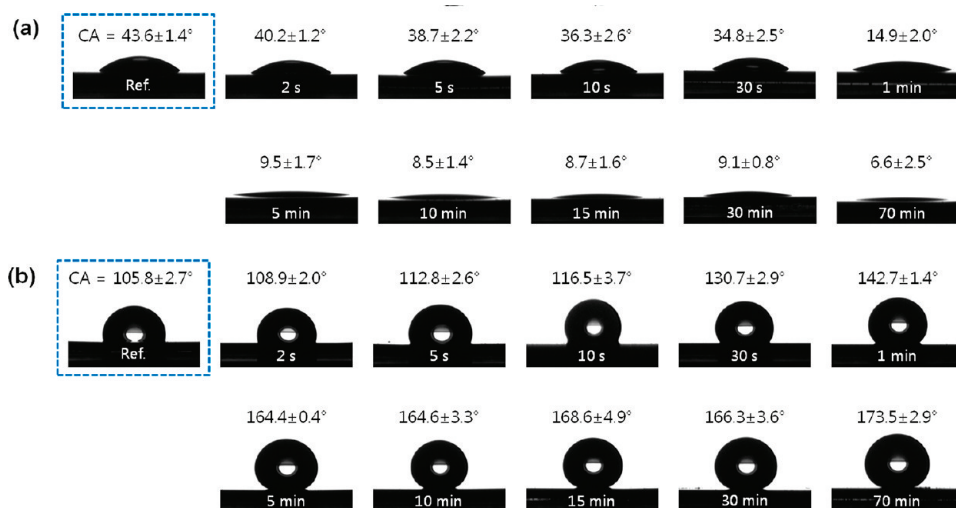

Figure 3. Apparent contact angles in relation to etching time for SiNWs and hydrophobic C_4F_8 layer (the blue dashed line represents a plain Si substrate without SiNWs): (a) effect of etching time on the surface roughness of intrinsic Si substrates without C_4F_8; (b) effect of etching time on Si substrates with a deposited C_4F_8 layer.

System) with the flow rate of C_4F_8 gas by 110 SCCM, RF power by 800 W, chamber pressure by 15 mTorr, and room temperature condition for substrate temperature.

Surface Morphology Characterization. In this study, the surface morphology was characterized by FE-SEM (JEOL-JSM-6700F), and the images are included in the main manuscript. The surface composition of the C_4F_8 layer was determined by energy dispersive X-ray spectroscopy (EDS) equipped with the same SEM. On the basis of our characterization by image processing, we determined the average height of the SiNWs, the distance between the SiNWs, and the diameter of the SiNWs.

Wettability Characterization. The surface contact angles on the fabricated substrates were determined using a contact angle measurement system (KSV CAM-200, KSV Ins.). Using images taken with a high speed camera with a frame interval of 2 ms and a resolution of 512 × 480 pixels, contact angles were analyzed by an automated imaging process based on the calibrating program. We measured the contact angles using a high speed camera with 2 ms frame interval, therefore it was possible to present the momentary droplet images when the DI water droplet was collided on the surfaces. Using a DI water droplet of about 2.5 μL, more than four sets of measurements were taken at different locations on the fabricated substrates and then averaged.

RESULTS AND DISCUSSION

Figure 1 shows a schematic of the overall fabrication processes for manipulating surface roughness and SFE. Using the EE method, we synthesize length-varying SiNWs by controlling the etching time from 2 s to 70 min. The aqueous etching solution consists of a mixture of 0.02 M $AgNO_3$ and 5 M HF. Figure 2 shows field emission scanning electron microscope photographs of the resulting modified silicon surfaces and illustrates the relationship between SiNW height and etching time. Even when the etching time is quite short, the etching process, which consists of electroless deposition of silver ions on a silicon substrate, followed by etching of the substrate with hydrofluoric acid, creates a rough surface with primitive SiNWs. As the etching time increases, SiNWs with increasing heights are clearly visible. By applying image processing to the SEM images, we estimated that the average height of the SiNWs had a linear relationship with etching time, with an etching rate of about 220 nm/min. This is in good agreement with the results of Srivastava et al. (linear relationship with an etching rate of about 250 nm/min).[41]

To control the wetting characteristics, the surface roughness of the silicon substrate is manipulated by controlling the heights of the SiNWs. We create superhydrophilic surfaces on bare silicon wafers with high SFE, and superhydrophobic surfaces by applying a fluorine carbon (C_4F_8) coating (20 nm thickness) to the samples with SiNWs using PECVD. The C_4F_8-coated silicon substrates have SFE lower than that of intrinsic Si without a coating layer. Figure 3a shows the apparent contact angle measurements of various surfaces, including intrinsic Si substrates, substrates with SiNWs, and substrates coated with C_4F_8. The bare Si substrate exhibits hydrophilic behavior with a static contact angle of 43.6°,[5] and the apparent contact angle decreases as the etching time increases for higher SiNWs. For samples with etching times longer than 5 min, liquid droplets spread out over the rough surfaces with SiNWs, indicating contact angles below 10°. The images present the momentary droplet captured by high speed camera with 2 ms frame intervals when the DI water droplet was collided on the surfaces. After a few second, the contact angle become near 0 degrees due to the superwetting or the hemiwicking phenomenon on the surfaces with silicon nanowire arrays which increase surface roughness sufficiently. On the other hand, the intrinsic Si substrates coated with C_4F_8 exhibit hydrophobic properties with a contact angle of 105.8°, which progresses toward the superhydrophobic regime with increasing SiNW height, as shown in Figure 3b. The contact angle transition from the hydrophilic to hydrophobic regime is related to SFE manipulation of the Si substrate. As previous research has shown,[35] whether a surface is hydrophilic or hydrophobic is dependent on the SFE of the initial substrate. General polymeric materials, including fluorine−carbon species, such as CF_2, CF_3, and C_4F_8 are known to have very low SFE values compared with metals or silicon.[42−44] Using the van-Oss method,[45−47] we verify that the SFE values of the intrinsic Si and the C_4F_8 coated Si substrate are 52.96 and 13.51 mJ/m^2, respectively. Thus, applying a C_4F_8 coating to a Si substrate

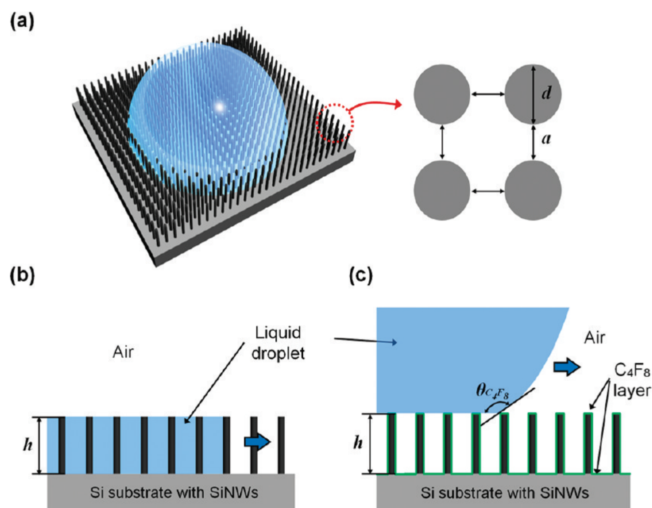

Figure 4. Diagrams of a liquid droplet on the modified surface: (a) liquid droplet and SiNWs on Si substrate; (b) liquid spreading through SiNWs, based on the hemiwicking phenomenon; (c) liquid droplet on the SiNWs according to the Cassie–Baxter model.

effectively decreases the wettability, because of the reduction of the SFE to a quarter (74.5% reduction) compared with the original value, and converts the hydrophilic into hydrophobic characteristics.

Figure 4 shows diagrams of liquid behavior on Si substrates with SiNWs. On the basis of previous researches[37,41] and the SEM images of Figure 2, we model densely distributed SiNWs on a substrate as uniformly distributed circular pillars in a local area, and a liquid droplet on the surface is illustrated in Figure 4a. For the bare Si substrate, which has high SFE and a hydrophilic contact angle less than 90°, the effect of surface roughness on the contact angle can be explained by Wenzel's relationship[48]

$$\cos\theta = r\cos\theta^*, \quad r = 1 + \frac{\pi dh}{(a+d)^2} \tag{1}$$

where θ is the apparent contact angle actually measured on the surface, r is a roughness factor, defined as the ratio of the actual surface area to the projected one, and θ^* is the equilibrium contact angle on an ideal plain surface. Here, the roughness factor is expressed in terms of the geometry of the pillar structures that represent SiNWs, as shown in Figure 4. It is a well-known consequence of Wenzel's relationship that the surface becomes more hydrophilic as the surface roughness increases in the hydrophilic regime ($0° < \theta^* < 90°$). In Figure 3a, it is shown that the contact angle decreases gradually with increasing SiNW height, ultimately reaching a superhydrophilic angle of less than 10°. If a hydrophilic surface has densely distributed textured micronanoscale structures, the hemiwicking phenomenon occurs.[35] In a hemiwicking regime, a water droplet should be absorbed and propagated outward by increasing the wetting area on the substrate. When a droplet progresses through the SiNWs, as shown in Figure 4b, the force balance at the boundary of the droplet between the intermediate fluids (liquid and gas phase materials) and the surface can be expressed as follows:

$$dF/dx = (\gamma_{SL} - \gamma_{SV})(\gamma - \varphi) + \gamma_{LV}(1-\varphi) \tag{2}$$

where γ_{SL}, γ_{SV}, γ_{LV}, and φ are the surface tension between the solid and liquid phase, solid and vapor (air), liquid and vapor, and the solid fraction remaining dry (that is, the top area fraction of the circular pillar structure in Figure 4b, $\varphi = \pi d^2/[4(a+d)^2]$, respectively. In eq 2, the first term on the right-hand side indicates an interaction between the liquid and the solid surface wetted by the liquid, and the second term represents an interaction between the air and the top surface of the pillars that are not wetted by the liquid. Based on Young's relationship ($\gamma_{LV}\cos\theta^* = \gamma_{SV} - \gamma_{SL}$) and eq 2, the analytical critical angle, θ_c, as a threshold value to induce the hemiwicking phenomenon, can be derived when $dF/dx < 0$. Thus, the apparent contact angle decreases within the superhydrophilic regime, when the prerequisite condition of superhydrophilic surface is satisfied as follows:

$$\cos\theta^* > \frac{1-\varphi}{r-\varphi}, \quad \cos\theta_c = \frac{1-\varphi}{r-\varphi} \tag{3}$$

Figure 5a shows the relationship between the apparent contact angles and critical angles according to the Si etching time variation in the synthesis process that produces the variation in SiNW height. The critical contact angle increases markedly as the etching time increases, and this is attributed to the rapid increase in the surface roughness due to increasing SiNW height h, described by eq 2. For the sample synthesized for 60 s, the analyzed critical angle is close to the value of θ^* for a plain Si substrate, while the critical value is much larger than θ^* for the samples with etching times longer than 60 s. As Figure 3 (a) indicates, a liquid droplet is readily absorbed and propagates through the SiNWs when the surface is superhydrophilic, due to the extremely rough surface morphology created by SiNWs. However, even though the surface roughness is adequate to satisfy the condition for superhydrophilicity, in view of the hemiwicking phenomenon, the contact angle does not converge to zero degrees as predicted by the original Wenzel relation (eq 1).[35] (Details are explained in the Supporting Information.)

In contrast to this, Si substrates with SiNWs can also be given superhydrophobic characteristics by increasing the roughness factor and lowering the SFE with a C_4F_8 layer. By lowering the SFE of the outer surface, which has a high roughness because of the vertical SiNWs, it is possible to prevent the transition of a liquid droplet from the Cassie–Baxter state to the Wenzel state, while maintaining thermodynamic stability in the air cavities formed on the substrate among the densely distributed SiNWs. In the hydrophobic regime with contact angle exceeding 90° (Figure 4c), the force variation per unit length can be expressed as follows:

$$dF/dx = \varphi(\gamma_{SL} - \gamma_{SV}) + (1-\varphi)\gamma_{LV} + \gamma_{LV}\cos\theta \tag{4}$$

where φ is the solid fraction of the solid/liquid contact area below the droplet in Figure 4c, which represents the same area fraction with the case of hydrophilic situation. In the Wenzel regime, the droplet sinks into the air cavities and contacts the sidewalls of the SiNWs. The criterion for transition from the Cassie–Baxter regime to the Wenzel regime can be obtained by comparing eq 4 (for the Cassie–Baxter state with varied forces) to eq 5 (for the corresponding Wenzel state) as follows:

$$dF/dx = r(\gamma_{SL} - \gamma_{SV}) + \gamma_{LV}\cos\theta \tag{5}$$

When the force variation derived by Cassie-state is less than that by Wenzel state (eq 2), air cavities could be maintained stably

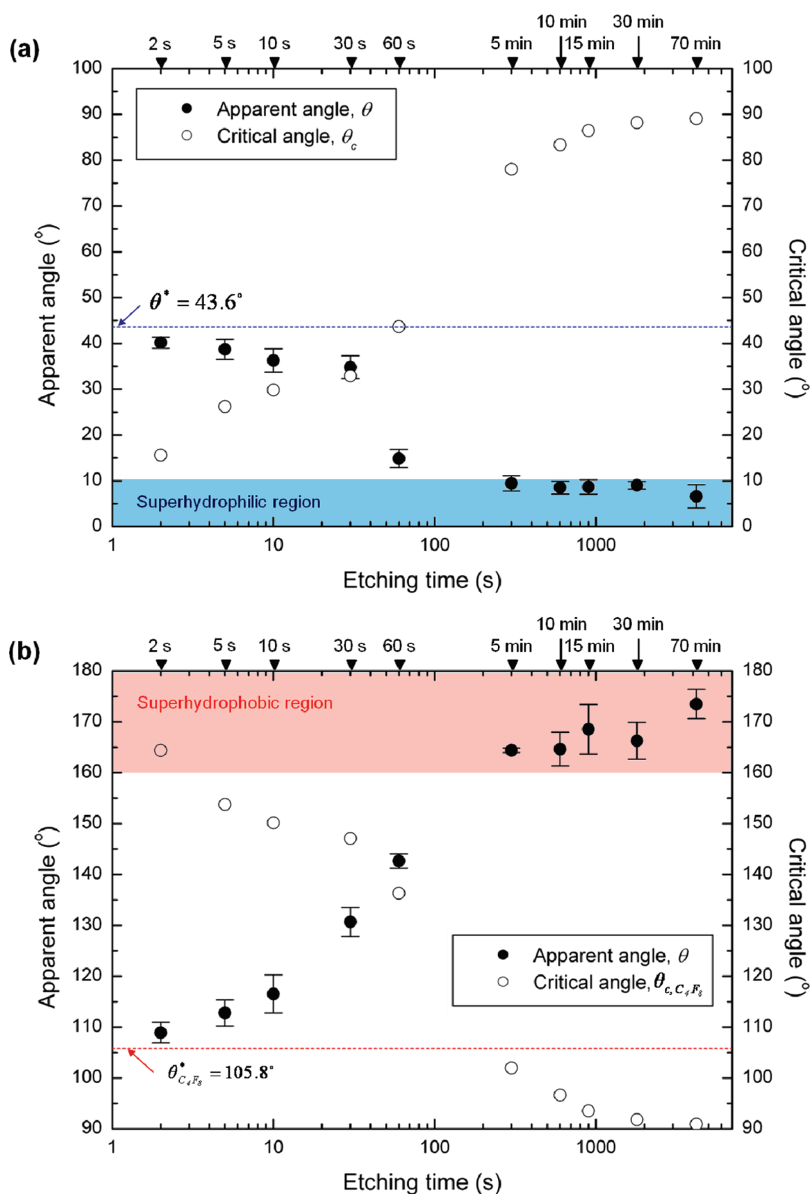

Figure 5. Apparent contact angles on surfaces with SiNWs and dependence of wettability on the relationship between the ideal contact angle of plain Si and critical contact angles according to variation of SiNW height: (a) for under superhydrophilic conditions; (b) under superhydrophobic conditions created by C_4F_8 deposition. Based on the SEM images, values of a_{avg} = 200 nm, and d_{avg} = 100 nm were used in the analytical criteria.

below the liquid droplet within porous space. Here, another critical contact angle, θ_{c,C_4F_8}, as a threshold value for the condition of stable air-cavity is expressed as follows:

$$\cos \theta^*_{C_4F_8} < \frac{\varphi - 1}{r - \varphi}, \quad \cos \theta_{c,C_4F_8} = \frac{\varphi - 1}{r - \varphi} \tag{6}$$

where the subscript C_4F_8 represents the C_4F_8-deposited condition. To obtain superhydrophobicity, the air cavities must be stably maintained to prevent wetting of the solid surface by a liquid. Equation 6 is a prerequisite criterion for superhydrophobicity. Figure 5b shows the relationship between the critical and apparent contact angles for SiNWs coated with C_4F_8. Because the roughness factor expressed in eq 2 increases markedly with SiNW height, the contact angle becomes more hydrophobic. When the theoretical criterion based on the Cassie–Baxter model for the required stability of the air cavities among the SiNWs is satisfied ($\theta_{c,C_4F_8} < \theta^*_{C_4F_8}$), superhydrophobic characteristics are clearly observed, with a contact angle exceeding 160° (from Figures 3b and 5b). In addition we evaluated the surface robustness of a superhydrophobic surface by applying pressure on the surface by pressing a droplet using micropipet attached on an automatically controlled traverse (in the Supporting Information).

Based on the theoretical analyses for critical angles and the experimental verifications in both hydrophilic and hydrophobic regimes, we can explain the influence of the surface roughness and the surface free energy for superhydrophilicity and superhydrophobicity like Figure 5, panels a and b, respectively. Based on SEM imaging, we confirmed that the conformal coating of 20 nm-thick C_4F_8 layer did not induce any formation of film/particle-like shapes by itself or coalescence of SiNWs anywhere because the coating thickness is relatively thin and the nanowires

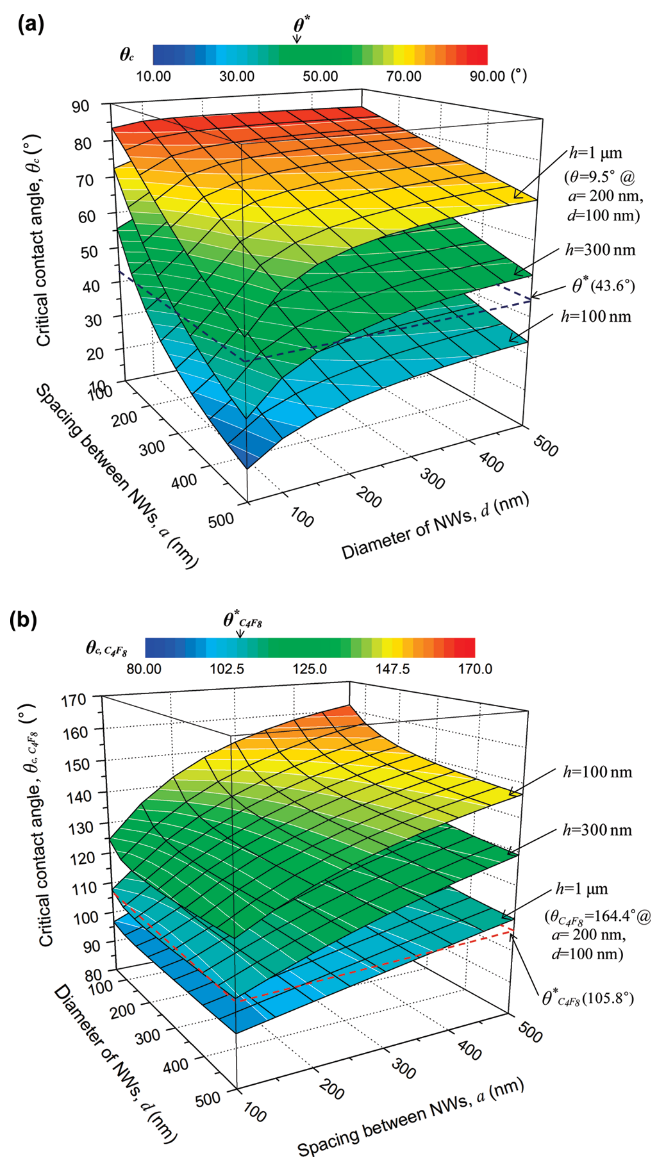

Figure 6. Surface distributions of the critical contact angle according to the variation of the geometric variables a (100−500 nm), d (50−500 nm), and h (100 nm, 300 nm, and 1 μm) of the SiNWs: (a) for superhydrophilic surfaces; (b) for superhydrophobic surfaces.

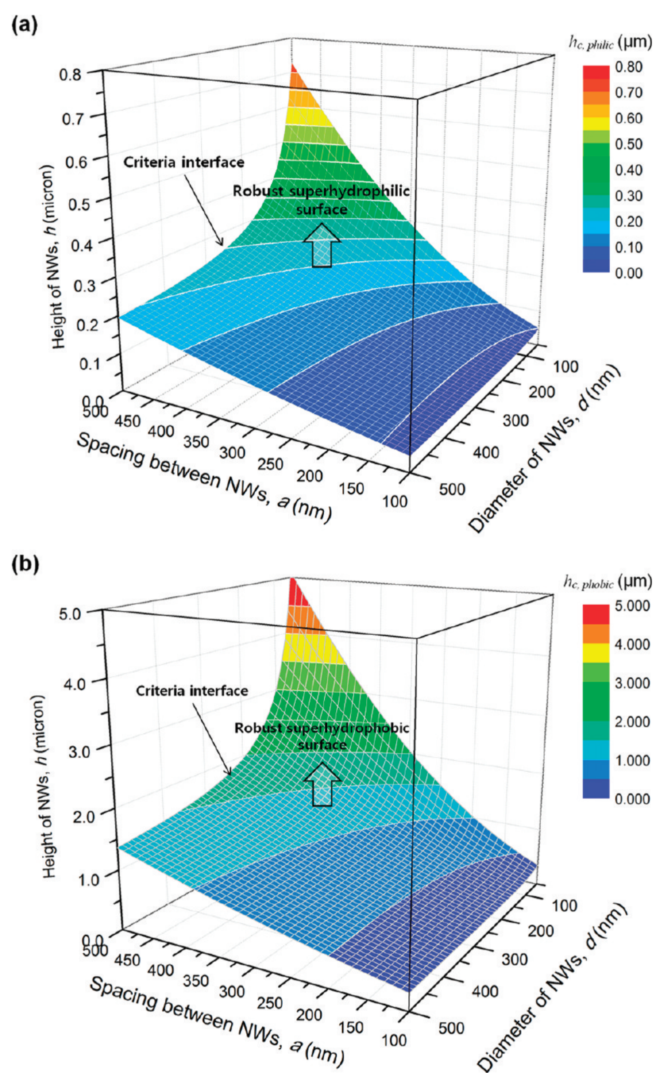

Figure 7. Contour maps describing the minimum value of h in terms of the variation of the geometric dimensions a and d and dimensional guideline ranges for robust design: (a) for a superhydrophilic surface; (b) for a superhydrophobic surface.

are separated from each other by distances of up to hundreds of nanometers.[26]

Other dimensional factors of SiNWs, such as the spacing (a) between those and their diameter (d) as well as their height (h) (depicted in Figure 4) can affect wettability criteria. Figure 6, panels a and b, show maps of the analytical criteria for the superhydrophilic and superhydrophobic regimes in terms of nanoscale a and d, with h in the range of 100 nm to 1 μm. It is necessary that the SiNWs have nanoscale lateral dimensions (a and d) to significantly increase the roughness factor, and increasing the height from nanoscale to micrometer order is particularly effective for satisfying the criteria for superhydrophilicity and superhydrophobicity. While it has been shown that variation of a and d also affects the critical contact angles, controlling h is much more powerful and effective in view of practical modification processes. As Figure 6 (a) indicates, when h is greater than a micrometer, the conditions for a superhydrophilic surface is satisfied ($\theta_c > \theta^* \sim 43.6°$) regardless of a and d. Values of h less than a micrometer fall short of the requirement for a superhydrophobic surface ($\theta_{c,C_4F_8} < \theta^*_{C_4F_8} \sim 105.8°$), and hence the height of the SiNWs must be appropriately increased in this case. Although it is possible to intentionally change a and d by adding an additional process (such as sphere lithography) to the EE method, more cost and effort are involved than in the simple EE method.[49,50] In view of the feasibility and simplicity of the EE method, superhydrophilic/superhydrophobic surfaces should be created primarily by manipulating h rather than the lateral dimensions a and d.

For manipulating wettability, the critical heights $h_{c,philic}$ and $h_{c,phobic}$ (the minimum values required for robust superhydrophilic and superhydrophobic surfaces) can be described as functions of the geometric variables and the ideal contact angle. Especially for superhydrophobicity, considering contact angle transition from Cassie-state to Wenzel-state, it is possible to obtain robust surface when there is minimal change in the apparent contact angle (between

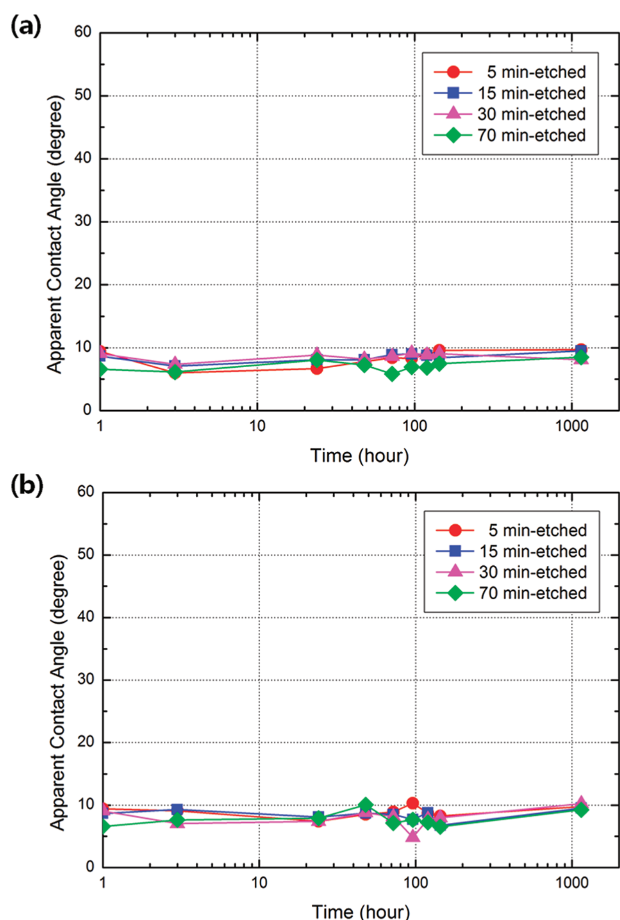

Figure 8. Time-dependent stability on the superhydrophilic surfaces: (a) SiNWs without C_4F_8 layer exposed in air; (b) SiNWs without C_4F_8 layer immersed in DI water.

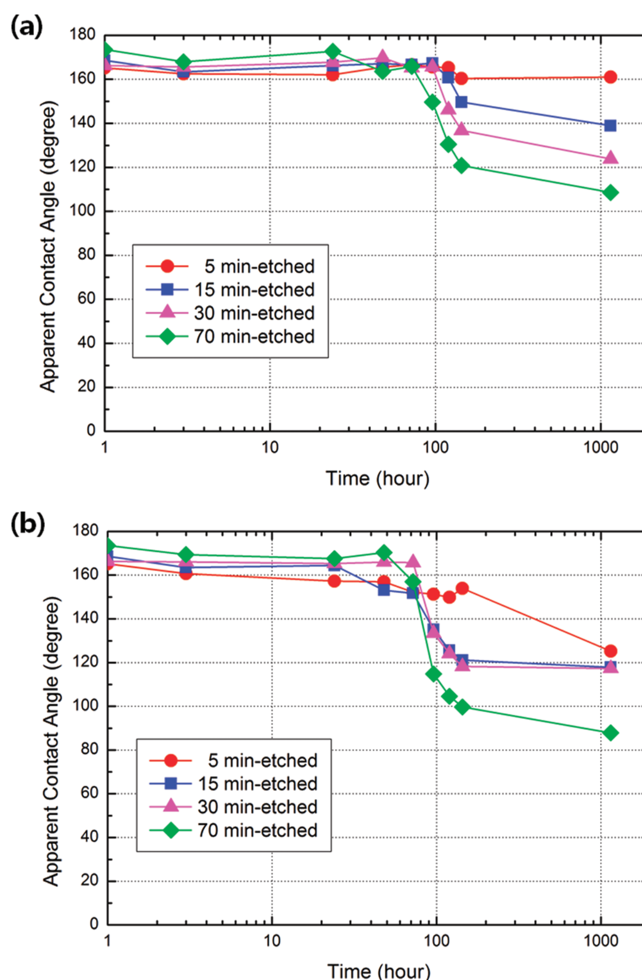

Figure 9. Time-dependent stability on the superhydrophobic surfaces: (a) SiNWs with C_4F_8 coated layer exposed in air; (b) SiNWs with C_4F_8 coated layer immersed in DI water.

contact angles estimated by Wenzel's model and Cassie's model) when the drop transition from Cassie to a Wenzel contact. Based on the analytical relationships between the critical angles and the equilibrium contact angles on a plain surface (eqs 3 and 6), we propose the following two criteria as design guidelines:

$$h_{\text{c, philic}} > \frac{1}{\pi d}\left(\frac{1}{\cos\theta^*} - 1\right)(1-\varphi)(a + d)^2 \tag{7}$$

$$h_{\text{c, phobic}} > \frac{1}{\pi d}\left(\frac{1}{\cos\theta^*_{C_4F_8}} + 1\right)(\varphi - 1)(a + d)^2 \tag{8}$$

For silicon substrates with SiNWs, with and without C_4F_8 coating, these values are shown in Figure 7. The 3-dimensional contour surfaces describe the minimum value of h in terms of the variation of the geometric dimensions a and d. Both $h_{\text{c,philic}}$ and $h_{\text{c,phobic}}$ must be increased when a increases, because increasing this factor diminishes the surface roughness. However, it could be seen that the critical heights are comparatively nonsensitive to the diameter d except the region with very low d (<100 nm). From the distribution of critical height for robust superhydrophilic (Figure 7a) and superhydrophobic surfaces (Figure 7b), it is possible to present the critical dimensions of nanoscale structures. The design domain with higher h value than that on the contour surfaces corresponds to the allowable region for robust superhydrophilic and superhydrophobic surfaces, respectively. From Figure 7, we can demonstrate that it is necessary to increase h to more than several hundred nanometers for a superhydrophilic surface and to more than a few micrometers for a superhydrophobic surface. Moreover, to facilitate wettability manipulation, we recommend carefully designed SiNWs rather than overetched nanowires with excessive height, which could fracture easily in response to fluid behavior or external impact.

Long-term stability of the superhydrophilic/superhydrophobic surfaces is another important aspect for the robustness of the surfaces.[17,26,51] Figure 8 presents the long-term stability results of the fabricated superhydrophilic surfaces under various environments. For superhydrophilic surfaces (Figure 8, panels a and b), contact angles maintain their own wetting property and wicking behavior with contact angles below 10° even after more than one month. Intrinsic silicon surface including a substrate and nanowire structures would oxidize creating hydrophilic SiO_2 layer by exposing the samples in air or in DI water although the environment makes difference in oxidizing process rate. This induces the relative good long-term stability for superhydrophilic surfaces as

presented in Figure 8, panels a and b. Therefore for the superhydrophilic surfaces via vertically aligned SiNWs synthesized by electroless silicon wet etching method, it seems to maintain manipulated superhydrophilicity sufficiently with more than 1 μm-height SiNWs in terms of long-term stability.

On the other hand, contact angles on the superhydrophobic surfaces (Figure 9, panels a and b) decrease with increasing exposed time in both air and DI water due to oxidization of Si substrate and SiNWs. For the samples exposed in air, superhydrophobic behavior is maintained for over a month on 5 min-etched samples. However, others do not have sufficient stability more than 4 days. Especially, contact angle degradation is greater on the samples immersed in DI water than those exposed in ambient environment. Although we coated the surface with conformal 20 nm-thick C_4F_8 polymeric layer, the polymeric material may not have been deposited on the whole area of the nanoscale structure surface. Therefore partially formed SiO_2 on the surface where the C_4F_8 material was not deposited would decrease contact angle due to its hydrophilic characteristics. For the samples immersed in DI water, contact angles decrease more remarkably than those exposed in air. This is because it is possible to expedite the oxidization of the substrate (Si) and SiNWs in water.[26] Considering the oxidization, it is possible to enhance the long-term stability of superhydrophobic surfaces by increasing the thickness of the polymeric layer to prevent silicon substrate and SiNWs from being exposed in air or DI water. This is because the exposed silicon surface is a main factor to cause the degradation of hydrophobicity. In addition, not only the oxidation of the surface but the degradation of average surface free energy by exposed silicon area would probably act as another factor to lower the time-dependent stability especially for superhydrophobicity. In this study for the superhydrophobic surfaces via SiNWs, we deposited relatively thin (conformal 20 nm-thick) hydrophobic polymer (C_4F_8) layer on the synthesized structures. As our future work, the thickness of the polymeric layer would be evaluated as another potential parameter on the stability of superhydrophobicity.

CONCLUSIONS

In conclusion, it is possible to manipulate the surface wettability of a Si substrate from the hydrophilic regime to the hydrophobic regime, using a C_4F_8 coating to lower the SFE to about 25.5% (13.51 mJ/m^2) compared with intrinsic Si (52.96 mJ/m^2). Prior to this coating, the EE method is used to maximize surface roughness by creating densely distributed vertical SiNWs with high aspect ratio. Surface roughness permits hydrophilicity or hydrophobicity to be increased to the extreme, according to the intrinsic wettability, determined by the SFE characteristics of the base substrate. Making use of the equations for the hemiwicking and Cassie−Baxter states, we demonstrate the criteria for superhydrophilic and superhydrophobic conditions, and present design guidelines as a function of the geometric variables of SiNWs. In addition, we evaluate long-term stability characteristics for manipulated superhydrophilicity and superhydrophobicity. We conclude that SiNWs fabricated with a height of more than a micrometer provide an effective means of obtaining superhydrophilic (<10°) and superhydrophobic surfaces (>160°). Considering the simplicity and feasibility of the fabrication process, the wettability modulation technique and guidelines developed in this study should be useful for designing various Si-based devices.

ASSOCIATED CONTENT

Supporting Information. Additional experimental details including supplimental videos. This material is available free of charge via the Internet at http://pubs.acs.org.

AUTHOR INFORMATION

Corresponding Author

*Tel.: +82 2 2123 2828. Fax: +82 2 312 2159. E-mail: hhcho@yonsei.ac.kr.

ACKNOWLEDGMENT

This work was supported by a National Research Foundation of Korea (NRF) grant funded by the Korea government (MEST) (No. 2011-0000252 and No. 2011-0017673). B.S.K. is grateful for a Seoul Science Fellowship provided by the Seoul Metropolitan Government.

REFERENCES

(1) Choi, C. H.; Ulmanella, U.; Kim, J.; Ho, C. M.; Kim, C. J. *Phys. Fluids* **2006**, *18*, 087105.

(2) Tuteja, A.; Choi, W.; Ma, M. L.; Mabry, J. M.; Mazzella, S. A.; Rutledge, G. C.; McKinley, G. H.; Cohen, R. E. *Science* **2007**, *318*, 1618–1622.

(3) Vourdas, N.; Tserepi, A.; Boudouvis, A. G.; Gogolides, E. *Microelectron. Eng.* **2008**, *85*, 1124–1127.

(4) Li, C.; Wang, Z.; Wang, P. I.; Peles, Y.; Koratkar, N.; Peterson, G. P. *Small* **2008**, *4*, 1084–1088.

(5) Chen, R.; Lu, M. C.; Srinivasan, V.; Wang, Z.; Cho, H. H.; Majumdar, A. *Nano Lett.* **2009**, *9*, 548–553.

(6) Phan, H. T.; Caney, N.; Marty, P.; Colasson, S.; Gavillet, J. *Int. J. Heat Mass Transf.* **2009**, *52*, 5459–5471.

(7) Byon, C.; Nam, Y.; Kim, S. J.; Ju, Y. S. *J. Appl. Phys.* **2010**, *107*, 066102.

(8) Shafiei, M.; Alpas, A. T. *Mater. Sci. Eng. C* **2008**, *28*, 1340–1346.

(9) Shibuichi, S.; Onda, T.; Satoh, N.; Tsujii, K. *J. Phys. Chem.* **1996**, *100*, 19512–19517.

(10) Wang, R.; Sakai, N.; Fujishima, A.; Watanabe, T.; Hashimoto, K. *J. Phys. Chem. B* **1999**, *103*, 2188–2194.

(11) Lau, K. K. S.; Bico, J.; Teo, K. B. K.; Chhowalla, M.; Amaratunga, G. A. J.; Milne, W. I.; McKinley, G. H.; Gleason, K. K. *Nano Lett.* **2003**, *3*, 1701–1705.

(12) Zhai, L.; Cebeci, F. C.; Cohen, R. E.; Rubner, M. F. *Nano Lett.* **2004**, *4*, 1349–1353.

(13) Hosono, E.; Matsuda, H.; Honma, I.; Ichihara, M.; Zhou, H. *Langmuir* **2007**, *23*, 7447–7450.

(14) Xiu, Y.; Zhu, L.; Hess, D. W.; Wong, C. P. *Nano Lett.* **2007**, *7*, 3388–3393.

(15) Patankar, N. A. *Soft Matter* **2010**, *6*, 1613–1620.

(16) Yuan, J. K.; Liu, X. G.; Akbulut, O.; Hu, J. Q.; Suib, S. L.; Kong, J.; Stellacci, F. *Nat. Nanotechnol.* **2008**, *3*, 332–336.

(17) Cebeci, F. C.; Wu, Z. Z.; Zhai, L.; Cohen, R. E.; Rubner, M. F. *Langmuir* **2006**, *22*, 2856–2862.

(18) Suzuki, T.; Kubo, K.; Hori, N.; Yamada, M.; Kojima, N.; Sugita, Y.; Maeda, H.; Ogawa, T. *Biomaterials* **2010**, *31*, 4818–4828.

(19) Tsougeni, K.; Papageorgiou, D.; Tserepi, A.; Gogolides, E. *Lab Chip* **2010**, *10*, 462–469.

(20) Wang, R.; Hashimoto, K.; Fujishima, A.; Chikuni, M.; Kojima, E.; Kitamura, A.; Shimohigoshi, M.; Watanabe, T. *Nature* **1997**, *388*, 431–432.

(21) Coffinier, Y.; Janel, S.; Addad, A.; Blossey, R.; Gengembre, L.; Payen, E.; Boukherroub, R. *Langmuir* **2007**, *23*, 1608–1611.

(22) Yeh, K. Y.; Chen, L. J.; Chang, J. Y. *Langmuir* **2008**, *24*, 245–251.

(23) Piret, G.; Coffinier, Y.; Roux, C.; Melnyk, O.; Boukherroub, R. *Langmuir* **2008**, *24*, 1670–1672.

(24) Kuan, W. F.; Chen, L. J. *Nanotechnology* **2009**, *20*, 035605.

(25) Niu, J. J.; Wang, J. N.; Xu, Q. F. *J. Nanosci. Nanotechnol.* **2009**, *9*, 1819–1824.

(26) Dai, Y. A.; Chang, H. C.; Lai, K. Y.; Lin, C. A.; Chung, R. J.; Lin, G. R.; He, J. H. *J. Mater. Chem.* **2010**, *20*, 10924–10930.

(27) Extrand, C. W.; Moon, S. I.; Hall, P.; Schmidt, D. *Langmuir* **2007**, *23*, 8882–8890.

(28) Ma, M. L.; Gupta, M.; Li, Z.; Zhai, L.; Gleason, K. K.; Cohen, R. E.; Rubner, M. F.; Rutledge, G. C. *Adv. Mater.* **2007**, *19*, 255–259.

(29) Tsougeni, K.; Tserepi, A.; Boulousis, G.; Constantoudis, V.; Gogolides, E. *Plasma Process. Polym.* **2007**, *4*, 398–405.

(30) Quere, D.; Lafuma, A.; Bico, J. *Nanotechnology* **2003**, *14*, 1109–1112.

(31) Patankar, N. A. *Langmuir* **2003**, *19*, 1249–1253.

(32) He, B.; Patankar, N. A.; Lee, J. *Langmuir* **2003**, *19*, 4999–5003.

(33) Tserepi, A. D.; Vlachopoulou, M. E.; Gogolides, E. *Nanotechnology* **2006**, *17*, 3977–3983.

(34) Chaudhury, M. K.; Whitesides, G. M. *Science* **1992**, *256*, 1539–1544.

(35) Bico, J.; Thiele, U.; Quéré, D. *Colloids Surf., A* **2002**, *206*, 41–46.

(36) Lafuma, A.; Quéré, D. *Nat. Mater.* **2003**, *2*, 457–460.

(37) Peng, K. Q.; Yan, Y. J.; Gao, S. P.; Zhu, J. *Adv. Mater.* **2002**, *14*, 1164–1167.

(38) Hochbaum, A. I.; Chen, R. K.; Delgado, R. D.; Liang, W. J.; Garnett, E. C.; Najarian, M.; Majumdar, A.; Yang, P. D. *Nature* **2008**, *451*, 163–168.

(39) Peng, K. Q.; Yan, Y. J.; Gao, S. P.; Zhu, J. *Adv. Funct. Mater.* **2003**, *13*, 127–132.

(40) Ayon, A. A.; Braff, R.; Lin, C. C.; Sawin, H. H.; Schmidt, M. A. *J. Electrochem. Soc.* **1999**, *146*, 339–349.

(41) Srivastava, S. K.; Kumar, D.; Singh, P. K.; Kar, M.; Kumar, V.; Husain, M. *Sol. Energy Mater. Sol. Cells* **2010**, *94*, 1506–1511.

(42) Hare, E. F.; Shafrin, E. G.; Zisman, W. A. *J. Phys. Chem.* **1954**, *58*, 236–239.

(43) Nishino, T.; Meguro, M.; Nakamae, K.; Matsushita, M.; Ueda, Y. *Langmuir* **1999**, *15*, 4321–4323.

(44) Seong, M. R.; Lee, G. Y.; Cho, S. H.; Lim, H. W.; Park, J. G.; Lee, C. S. *Jpn. J. Appl. Phys.* **2008**, *47*, 6422–6426.

(45) Van Oss, C. J.; Good, R. J.; Chaudhury, M. K. *Langmuir* **1988**, *4*, 884–891.

(46) Zhao, Q.; Liu, Y.; Abel, E. W. *J. Colloid Interface Sci.* **2004**, *280*, 174–183.

(47) Aulin, C.; Ahok, S.; Josefsson, P.; Nishino, T.; Hirose, Y.; Österberg, M.; Wågberg, L. *Langmuir* **2009**, *25*, 7675–7685.

(48) Wenzel, R. N. *Ind. Eng. Chem.* **1936**, *28*, 988–994.

(49) Huang, Z.; Shimizu, T.; Senz, S.; Zhang, Z.; Zhang, X.; Lee, W.; Geyer, N.; Gosele, U. *Nano Lett.* **2009**, *9*, 2519–2525.

(50) Peng, K. Q.; Wang, X.; Wu, X. L.; Lee, S. T. *Appl. Phys. Lett.* **2009**, *95*, 143119.

(51) Patel, P.; Choi, C. K.; Meng, D. D. *J. Assoc. Lab. Automat.* **2010**, *15*, 114–119.